VOCs conversion in He/H2O plasma produced in a microcapillary tube at atmospheric pressure

Gerard Bauville, Michel Heninger, Joël Lemaire, Pascal Jeanney, Joao Santos Sousa, Antoine Pallandre, Stéphane Pasquiers

To appear in Journal of Physics D: Applied Physics (2024)

VOCs conversion in He/H_2O plasma produced in a micro-capillary tube at atmospheric pressure

G. Bauville[1], M. Heninger[2], J. Lemaire[2], P. Jeanney[1], J. Santos Sousa[1], A. Pallandre[2] and S. Pasquiers[1]

[1] Université Paris-Saclay, CNRS, Laboratoire de Physique des Gaz et des Plasmas, UMR8578, 91405 Orsay Cedex, France
[2] Université Paris-Saclay, CNRS, Institut de Chimie Physique, UMR8000, 91405 Orsay Cedex, France

Corresponding author: stephane.pasquiers@cnrs.fr

Abstract
A non-equilibrium plasma is created in a micro-capillary quartz tube (800 µm of internal diameter), by a DC-pulsed micro-Dielectric Barrier Discharge (micro-DBD) and the propagation of an ionisation wave, in mixtures of He/H_2O/VOC at atmospheric pressure where the studied Volatile Organic Compounds (VOCs) are representative of molecules belonging to different chemical families: alcohols (methanol, ethanol, isopropanol, tert-butanol), ketones (acetone), nitriles (acetonitrile), and aromatic hydrocarbons (toluene). The conversion efficiency of these VOCs is studied as a function of the applied voltage on the micro-DBD (or electrical energy deposited in the plasma) and of the initial concentration of the molecules in the range from 1 ppm up to 3000 ppm (depending on the molecule), with the help of high-resolution real-time mass spectrometry CI-FTICR (Fourier Transform Ion Cyclotron Resonance associated to Chemical Ionisation) using H_3O^+ as precursor ion. A variety of by-products resulting from the conversion of VOCs are identified and quantified, emphasising that the micro-capillary plasma is able to induce a complex chemical reactivity. A qualitative analysis of the involved kinetics, based on the existing literature, reveals that helium species (ions and metastable states) and radicals coming from the dissociation of the water molecules (O and OH) are the most probable candidates to explain the formation of all compounds detected by the CI-FTICR apparatus. Quenching processes of the metastable He(2^3S) by the VOCs, leading to the dissociation of the molecules, are suggested to explain some of the experimental results.

Keywords: micro-discharge plasma, capillary tube, helium, water vapor, Volatile Organic Compounds, chemical ionisation mass spectrometry.

1. Introduction

Cold plasma micro-reactors, designed for example for chemical synthesis [1, 2] or the treatment of organic molecules in water [3], constitute a rapidly developing subject of study. This often involves using one or more dielectric barrier micro-discharge(s) (micro-DBD) to generate a plasma with high densities of reactive species, atoms, radicals or molecular excited states, which will initiate the physico-chemistry of interest for the envisaged application. The possibility of including a micro-DBD in a gas-liquid microfluidic system has been demonstrated, with important results for synthesis [1, 2]. DBDs have been also used for treatment of gaseous effluents (air) polluted by Volatile Organic Compounds (VOCs) in catalytic alveolar structures [4, 5]. In addition, research on cold plasma produced by pulsed electrical discharge generating a propagating ionization wave in capillary tubes attracts increasing attention, driven in particular by applications linked to analytical chemistry [6], or to health like for instance endoscopy [7], or transport of reactive species for the treatment of cancerous tumors [8]. Such plasma is also interesting for treating microchannel surfaces [9], whose coatings are essential to control transport phenomena and limit non-specific adsorption of analytes in labs on a chip.

A number of experimental and theoretical studies has been performed these last ten years on the physics of plasma produced in micro-capillary tubes, i.e. for tubes with an inner diameter in the millimetre size or much less (down to a few μm), using either RF [12], AC [16, 17], or DC-pulsed [10, 11, 13-15] electrical excitation. The vast majority of these works concerns helium and some of them argon, eventually with addition of a low concentration of oxygen molecules [18]. It brought important knowledge about the influence of the tube diameter on the discharge ignition and sustaining voltage, the propagation velocity of the ionization wave, and other important properties of the plasma such as the electric field in the streamer head, the produced electron density and the electron mean energy, as well as the plasma sheath within tubes for a better understanding of the plasma-surface interaction.

To the authors' knowledge, the effectiveness of a plasma produced by an ionization wave in a micro-capillary tube for the initiation of complex chemical reactions and the conversion or synthesis of organic molecules has not been studied until now. As a first step, the present study discusses the effect of a micro-capillary non-thermal helium plasma on some VOCs chosen for their different chemical nature. A DC-pulsed high voltage power supply was used to energize a micro-DBD producing the propagating ionization wave in the tube. Chosen molecules were, for concentration values in the range from 50 ppm up to 2500 ppm at atmospheric pressure: acetonitrile CH_3CN (representative of the nitrile family), acetone CH_3COCH_3 (ketone family), methanol CH_3OH, ethanol C_2H_5OH, isopropanol $CH_3CH(OH)CH_3$, and a representative of tertiary alcohols, tert-butanol $(CH_3)_3COH$; as representative of aromatic compounds, toluene $C_6H_5CH_3$ was also studied but at very low concentration values between 0.5 ppm and 5 ppm. In this work, we have not tried to study precisely the conversion of a particular VOC as a function of its initial concentration over a wide range of values. The aim was rather to evaluate the effectiveness of the micro-capillary plasma for a variety of compounds at some values of concentration for each, and with selected electrical parameters of the micro-DBD. For all of these compounds, water vapour was added to the gas mixture at a concentration of 2.5% (100% relative humidity); the basic idea was to benefit from the strong reactivity of the hydroxyl radical OH, coming from the dissociation of H_2O in the plasma, with organic molecules. However, the conversion of tert-butanol was also studied in a dry helium flow in order to get precise insight of the effect of the water vapour, concerning both the rate of conversion of the VOC and the by-products formed.

In order to get real-time monitoring of the different molecule concentrations, a compact permanent magnet Fourier Transform Ion Cyclotron Resonance (FTICR) mass spectrometer using chemical ionization (CI) was implement at the exit of the micro-plasma; this method diagnosis has proved to be very effective for studies of VOCs removal by plasmas [19-22]. Chemical ionization is a soft and selective ionization technique using ion/molecule reactions such as charge or proton transfers. The most used CI precursor ion is H_3O^+, which reacts with most VOCs with little fragmentation whereas it is nonreactive with the major components of the matrix, i.e. He for the present study. Consequently, a

compound with a molecular mass M will be detected at mass M+1 corresponding to (VOC)H+ ion. This technique is known as Proton Transfer Reaction Mass Spectrometry, PTR-MS [23]. It is currently used for academic research [24] or industrial applications [25]. As mentioned by several authors, PTR-MS is a promising tool for real-time analysis of trace organic by-products following the degradation of a VOC by a plasma process [26-29]. The analysis is quantitative if the reaction rate constant is known, that is the case for most common VOCs; if not known experimentally, the rate constant can be calculated from molecular properties [30]. For the present study, in addition to the conversion rates of the primary VOC in the mixture, PTR-MS allowed to precisely identify and quantify some by-products for acetonitrile, isopropanol, and tert-butanol.

2. Experimental set-up, electrical parameters and protocol for mass spectrometry

2.1 Set-up and short discharge characterisation

The micro-capillary tube (70 cm long) used in the experiment was made in quartz with inner/outer diameters respectively equal to 800/1000 µm. A stainless-steel needle was inserted inside the tube, whose outer diameter closely match the inner diameter of the tube so that it is placed in contact (glued) with the dielectric wall, and it was used as both the high voltage electrode and the gas inlet (inner diameter 400 µm). A copper tape (5 mm long) wrapped around the tube served as the counter-electrode connected to ground. The needle extremity was placed half long the copper tape (i.e. 2.5 mm from the tape end). This assembly is similar to what was previously designed for the generation of plasmas in rare gas micro-jets propagating into the ambient atmosphere [31, 32]. A schematic drawing of the overall experimental set-up is given in figure 1.

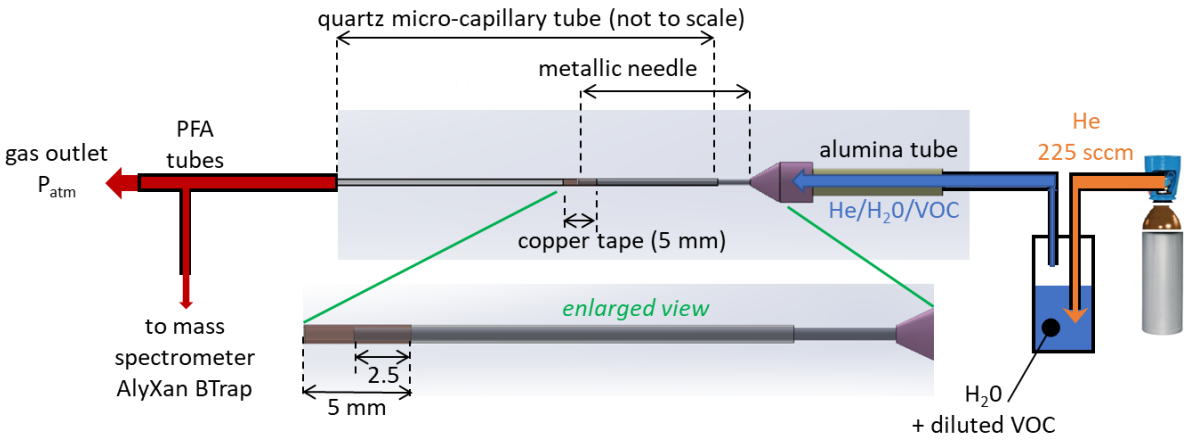

Figure 1 – Schematic drawing of the experimental set-up.

The gas flow inside the needle and further propagating in the quartz capillary was set to 225 sccm for all measurements, and at atmospheric pressure. In order to inject the mixture $He/H_2O/VOC$ in the tube, each organic molecule was separately dissolved in a water container (5% of liquid VOC) and helium (Alphagaz 2 quality from Air Liquide) was bubbled in the liquid mixture at room temperature, measured at around 21°C (±1°C). In such conditions the water vapor concentration was kept constant at 2.5% (±0.1%) for all studied mixtures. The obtained concentration of the chosen VOC in the gas flow was dependent on the molecule vapor pressure, see further in the article, but it did not exceed 3000 ppm. Without plasma in the micro-capillary and except for tert-butanol diluted in dry helium, we observed that the concentration of injected molecules decreased during time at a rate depending upon the type of compound diluted in the water container. The same decrease was observed during the discharge operation (see for example figure 4).

A high voltage (HV) pulse was applied on the metallic needle using a DC power supply (DEI model PVX-4110). The HV-pulse repetition frequency was fixed to 10 kHz, and the voltage amplitude was

varied from 1.5 kV up to 8.0 kV. The pulse duration was set to 3 µs, with pulse rising and falling times equal to 50 ns. Current and voltage waveforms were measured by means of electrical probes (Lecroy PPE20kV, Bergoz CT-B5-0.5) connected to a fast digital oscilloscope (Lecroy HDO 6104, 1 GHz). Examples of electrical measurements are presented in figure 2 for pure helium; such time evolutions are qualitatively similar for all gas mixtures and all voltage values chosen.

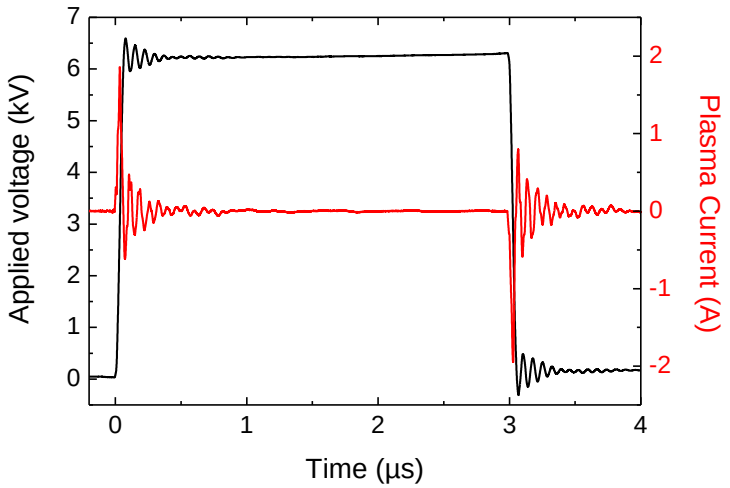

Figure 2 – Examples of time evolutions of applied voltage and plasma current (pure helium).

The plasma current was obtained after substraction of the displacement current (with an estimated capacitance of 2.0 pF) from the total signal provided by the probe. The figure 2 emphasises that the plasma is created both during the rising edge and during the falling edge of the HV-pulse. The current oscillations at the beginning of the pulse are damped in a few hundred nanoseconds, and no current is measured during the time interval [1 µs, 3 µs] which should correspond to a post-discharge afterglow with electron-ion recombination processes. The plasma created at the falling edge of the HV-pulse can be understood as a second discharge in the micro-capillary tube, whose establishment benefits from the residual electrical charges of the first discharge (rising edge of HV-pulse) and the creation of new charges during the high voltage plateau by Penning collisions of the helium metastable states.

The electrical energy deposited in the plasma during each HV-pulse was determined through time integration of the instantaneous electrical power defined as the product of the applied voltage times the absolute value of the plasma current. This energy is a quasi-linear increasing function of the applied voltage, with a maximum of 1.4 mJ at 8.0 kV. About 90% (or 80%) of the energy is deposited during the rising edge of the voltage for the wet mixture (or dry helium).

On top of that, the length of the plasma created in the tube, i.e. the propagation length of the ionisation wave, was measured using a digital camera (CoolSNAP from Photometrics). Figure 3 shows the plasma length for pure helium as well as for the mixture $He/H_2O(2.5\%)$, as a function of the deposited energy per HV-pulse.

To appear in Journal of Physics D: Applied Physics (2024)

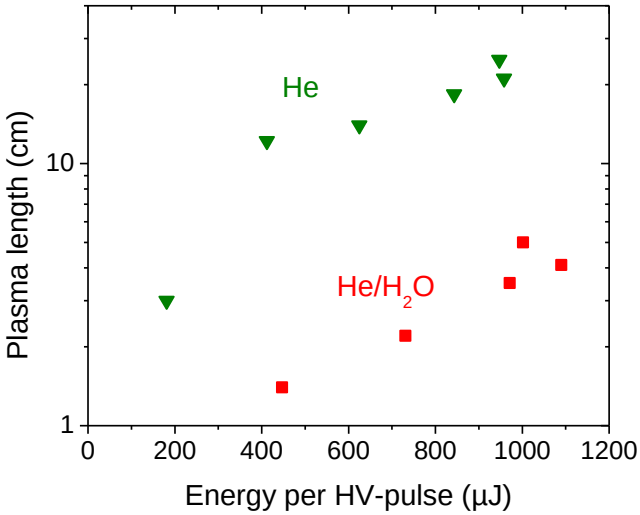

Figure 3 – Plasma length in the micro-capillary tube for pure helium and for the mixture He/H_2O(2.5%).

It can be seen that, at a fixed energy per pulse, the plasma length decreases sharply when water vapor is added to helium. In addition, we have established that adding a VOC to He/H_2O(2.5%) did not change the plasma length. More experiments are planned to get a better understanding of the effect of the water vapor on the plasma characteristics, this issue being not the subject of the present paper.

2.2 BTrap mass spectrometer, sampling and quantification

The BTrap instrument (from the company AlyXan, France) has already been described elsewhere [33, 34]. Briefly it is a FT-ICR mass spectrometer based on a permanent magnet assembly that produces a 1.5 T magnetic field. The ICR cell is derived from a cubic cell but has an open geometric structure that allows a good pumping and is well suited for the pulsed introduction of gases.

Ionization is done by chemical ionization in the ICR cell. In this study the precursor ions used are H_3O^+ ions. They are prepared by electron impact on a pulse of water vapor and then interact with the pulse of sample gas. H_3O^+ reacts with the VOCs present in the sample by proton transfer,

$$H_3O^+ + M \rightarrow H_2O + MH^+ \qquad (1)$$

and it reacts with H_2O but to reproduce the ion (symmetric charge transfer),

$$H_3O^+ + H_2O \rightarrow H_2O + H_3O^+ \qquad (2)$$

but it does not react with the carrier gas, helium.

The gas mixture is sampled at the exit of the micro-capillary and only a small fraction of the flow goes to the mass spectrometer. The drop from atmospheric pressure to a few 10^{-5} mbar is done in two steps: a first drop to a few mbar is done through a leak valve associated with a primary pump and the second drop occurs through a capillary of 100 µm internal diameter. In order to ensure a continuous gas flow and a good response time of the analyser, a three-way valve is used to direct the flow either to the vacuum chamber housing the ICR cell (pumped by a turbomolecular pump) or to an auxiliary vacuum chamber (also pumped by a turbomolecular pump).

The measurement by the mass spectrometer is repeated every 2 seconds. The mass spectrum is obtained by Fourier Transformation. VOCs are identified from the mass over charge ratio of the protonated ions formed and their concentration, [M], is obtained using the following quantification formula [34]:

$$[M] = \frac{\ln\left(\frac{Sum}{I_{H_3O^+}}\right).I_{MH^+}.10^6}{\left(Sum - I_{H_3O^+}\right).k_M.Pt.3.21} \qquad (3)$$

where I_{H3O+} and I_{MH+} are the intensities of the H_3O^+ and MH^+ ions and 'Sum' is the sum of the intensities for all the ions. 'Pt' is the pressure of the sample pulse integrated over time, and k_M is the rate coefficient of the protonation reaction (1). Mass spectra are averaged over 10 measurements, so that concentration values of molecules are deduced every 20 seconds (see figures 4 and 6).

For the tert-butanol, the reaction of the molecule with H_3O^+ produces two ions at masses 57 u (raw formula $C_4H_8^+$) and 75 u ($C_5H_{10}O^+$) [35], thus values given in the followings correspond to the sum of concentrations deduced from signals acquired on these two masses.

3. Results of PTR mass spectrometry

In the following are presented the experimental results concerning the concentrations of molecules at the exit of the plasma for a gas mixture containing water vapour, and in the case of tert-butanol also in the dry mixture with He. These results are discussed further in part 4 with respect to probable involved kinetics.

We define the conversion rate of a molecule by the ratio $(C_{in}-C_{out})/C_{in}$ (given in % in the following tables) where C_{in} and C_{out} are the inlet and outlet concentration values, respectively. For all molecules studied, the conversion rate depends upon the applied voltage (or the deposited energy) for a given value of C_{in}, and upon C_{in} for a fixed applied voltage (energy): the lower the inlet concentration or the higher the voltage, the higher the rate. These effects are comparable to those observed for the conversion of VOCs in mixtures of atmospheric gases and various types of pulsed discharges [36], although kinetic processes involved should be different.

It should be noted that not all by-products following the decomposition of the injected molecules were detected by PTR-MS with the use of the hydronium ion, in particular saturated hydrocarbons. The present work was not dedicated to an exhaustive characterization of these by-products.

3.1 Acetonitrile in the wet mixture

As typical examples of measurements, figures 4A and 4B show the time evolution of the acetonitrile concentration at the exit of the micro-plasma, for two values of the applied voltage, 3.0 kV and 5.0 kV respectively. In these experiments, the molecule inlet concentration was continuously decreasing at a rate of 9 ppm/min (fig.4A) and 78 ppm/min (fig.4B). The same decreasing rate was observed without or with operation of the micro-DBD. Thus, it was possible to determine the removal rate of the molecule for two different values of the inlet concentration, firstly, at the time of switching on the micro-DBD (t= 0 min), and secondly, at the time of switching off the discharge (t=7.5 min in figure 4A, t=6.5 min in figure 4B). This protocol was applied for all molecules diluted in the wet mixture $He/H_2O(2.5\%)$. In figure 4 for acetonitrile, the inlet concentration was, for 3.0 kV, C_{in}=316.9 ppm at t= 0 min, and C_{in}=203.7 ppm at t=7.5 min; for 5.0 kV, C_{in}=1903.0 ppm at t=0 min and C_{in}=1135.0 ppm and t=6.5 min; the corresponding outlet concentration values and the deduced removal rates are given in table 1.

To appear in Journal of Physics D: Applied Physics (2024)

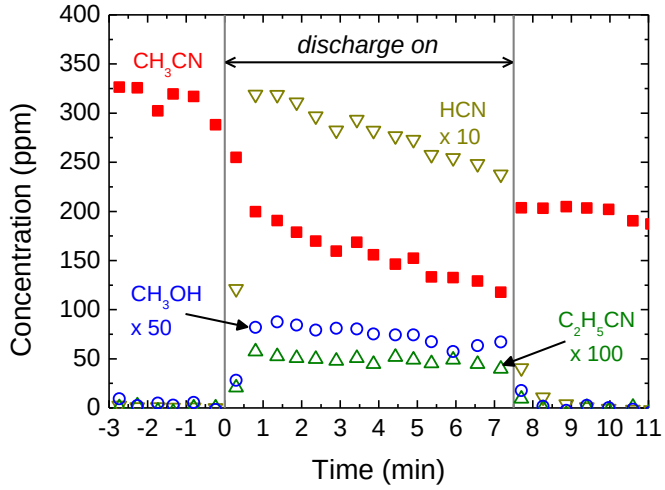

Figure 4A – Concentration of acetonitrile (full squares) as function of time for an applied voltage equal to 3.0 kV and an inlet concentration value of 316.9 ppm at the time of switching on the micro-DBD, together with those of three by-products (open symbols) magnified by a factor: 10 (HCN, down triangles), 50 (CH_3OH, circles), 100 (C_2H_5CN, up triangles).

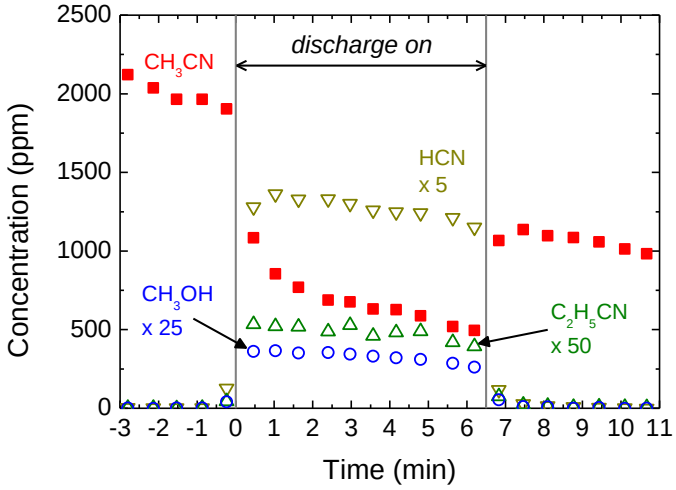

Figure 4B – Same as figure 4A, for an applied voltage equal to 5.0 kV and an inlet concentration value of 1903.0 ppm. Magnified factor for products: 5 (HCN), 25 (CH_3OH,), 50 (C_2H_5CN).

In table 1 are given all the conversion rates we were able to deduce from the PTR-MS measurements for CH_3CN, diluted in helium and for 2.5 % of water vapour, versus the inlet concentration and for different values of the applied voltage. Measurements are sorted in order of increasing inlet concentration. The voltage values were chosen in order to achieve the widest overview of the molecule conversion and the types and concentrations of the resulting by-products. For C_{in} ranging from 110 ppm up to 1900 ppm and voltage values between 2.0 kV and 6.0 kV, the obtained conversion rate lies between 23% and 81%.

Table 1. Conversion rate measured for acetonitrile (CH_3CN), diluted in the mixture $He/H_2O(2.5\%)$. (*): see figure 4A; (**): see figure 4B.

Inlet concentration (ppm)	Applied voltage (kV)	Outlet concentration (ppm)	Conversion rate (%)
109.7	4.0	21.0	80.9
190.9	4.0	50.1	73.8
203.7	3.0*	123.4	39.4
316.9	3.0*	199.5	37.0
501.4	2.0	387.8	22.7
640.0	6.0	189.0	70.5
951.0	6.0	278.0	70.8
1135.0	5.0**	494.0	56.5
1903.0	5.0**	854.0	55.1

Four by-products have been detected and quantified: hydrogen cyanide HCN, propane nitrile C_2H_5CN, methanol CH_3OH (concentration values given for example in figures 4), and acetone CH_3COCH_3 (not shown on the figures). The deduced carbon balance, simply defined as the ratio of detected C-atoms at the tube exit over injected ones, lies between 8% (for an applied voltage of 2.0 kV and C_{in} =501.4 ppm) and 26% (6 kV, 640.0 ppm). It emphasizes that the decomposition of acetonitrile induces the formation of other compounds than those detected with the use of H_3O^+. The most populated product is hydrogen cyanide. Concentration of this compound represents at minimum 10% (2.0 kV and C_{in}=501.4 ppm) and at maximum 48% (6 kV, 640.0 ppm) of the converted concentration of acetonitrile. Each of the others represents less than 2% for all conditions studied.

3.2 Ethanol, isopropanol and tert-butanol in the wet mixture

Except for methanol (see section 3.4), the measured conversion rates for the studied alcohols are given in table 2, versus the inlet concentration diluted in helium and for 2.5 % of water vapour, and for different values of the applied voltage. For each alcohol, measurements are sorted in order of increasing inlet concentration. Note that our experimental set-up led to higher C_{in} values for the tert-butanol than for the other alcohols.

Table 2 emphasises the following main results. For all alcohols at an inlet concentration lower than 1000 ppm, conversion rates of the order of 40% at least were achieved for a maximum applied voltage of 5.0 kV. A conversion rate higher than 90% was measured for ethanol and isopropanol at 5.0 kV and C_{in} in the range 90 ppm up to 335 ppm. For the same voltage, the efficiency of the plasma to convert the tert-butanol was even better, the conversion rate reaching more than 95% for an higher inlet concentration around 700 ppm (±50 ppm). However, for this molecule, the conversion rate was degraded when the inlet concentration was increased beyond 1000 ppm.

Table 2. Conversion rate measured for ethanol (C_2H_5OH), isopropanol ($CH_3C(OH)CH_3$), and tert-butanol ($(CH_3)_3COH$) diluted in the mixture $He/H_2O(2.5\%)$.

Molecule	Inlet concentration (ppm)	Applied voltage (kV)	Outlet concentration (ppm)	Conversion rate (%)
C_2H_5OH	135.6	3.0	24.5	81.9
	151.7	2.0	86.5	43.0
	187.6	2.0	112.5	40.0
	197.0	5.0	0.0	100.0
	332.8	5.0	18.3	94.5
$CH_3CH(OH)CH_3$	56.5	1.5	34.8	38.4
	69.1	2.0	27.8	59.8
	89.0	2.0	44.8	49.7
	89.3	5.0	0.7	99.2
	142.5	5.0	9.6	93.3
$(CH_3)_3COH$	676.5	5.0	9.1	98.7
	740.6	5.0	29.2	96.1
	1567.1	3.0	1308.4	16.5
	1854.2	3.0	1510.6	18.5
	2041.0	5.0	1441.0	29.4
	2510.0	5.0	1712.0	31.8

Detected by-products for ethanol were CH_3OH, CH_3CHO and CH_3COCH_3, and for isopropanol, we identified CH_3CHO and CH_3COCH_3. Unfortunately, it was not possible to quantify precisely concentrations of these compounds for all conditions listed in table 2. However, it was established clearly that the most populated one for ethanol was acetaldehyde. For example, about 50% of the C-atoms coming from the converted alcohol molecules were detected in this compound for a low applied voltage value of 2.0 kV and C_{in}=170 ppm (±20 ppm), whereas it was 30% in acetone, and only 5% maximum in methanol. On the other hand, acetone was the very main by-products for isopropanol. It represents for example more than 90% of the C-atoms at 2.0 kV and C_{in}=80 ppm (±10 ppm), whereas it was 5% maximum for acetaldehyde.

For the tert-butanol, up to eleven compounds were identified and quantified. As for isopropanol, acetone was the main one, with 21% up to 26% of the C-atoms coming from the converted molecules at all voltage values. For the other by-products, it does not exceed 4% for each. The deduced carbon balance is in the range 33% (at 3.0 kV and C_{in}=1854.2 ppm) up to 45% (5.0 kV, 2041.0 ppm), showing that, as for acetonitrile, the decomposition of the alcohol induces the formation of compounds which are not detected with H_3O^+ as precursor ions for the mass spectrometry.

Table 3 gives the list of detected compounds coming from the decomposition of $(CH_3)_3COH$, together with concentration values measured for an applied voltage of 5.0 kV and an inlet concentration of 2041.0 ppm. For this typical example, the converted concentration was 600.0 ppm. Most of the carbon atoms are found in acetone but other molecules with at least 3 C were also formed: 2-butanone, [hydroperoxide, 1-methylethyl], one compound which identification is suppositional, dimethyl ketene, a molecule containing seven C with a proposed raw formula C7H14O (see section 4.2.4 for possible compounds), and also two unsaturated hydrocarbons, propyne and propene. Four lighter molecules are also formed: methanol, formaldehyde, acetaldehyde, and ketene.

Table 3. Molecules detected from the decomposition of $(CH_3)_3COH$, with their concentration values, for an applied voltage of 5.0 kV and an inlet concentration of 2041.0 ppm diluted in the mixture $He/H_2O(2.5\%)$. '% C': percentage of carbon atoms coming from the converted tert-butanol molecules. (*): tentative interpretation for the detected ion mass MH^+=71.09 u. (**): raw formula attributed to the detected ion mass MH^+=115.09 u. The last column indicates presence of the molecules for the dry mixture (see section 3.3).

Molecule	Concentration (ppm)	% C	Dry mixture
CH_3COCH_3 – acetone	208.7	26.1	Yes
CH_2O – formaldehyde	42.8	1.8	No
CH_3OH – methanol	40.0	1.7	No
$C_2H_5COCH_3$ – 2-butanone	22.6	3.8	No
C_3H_6 – propene	16.4	2.1	Yes
CH_3CHO – acetaldehyde	13.1	1.1	Yes
C_3H_4 – propyne	12.6	1.6	Yes
C7H14O**	10.7	3.1	Yes
$(CH_3)_2CHOOH$ hydroperoxide, 1-methylethyl	10.6	1.3	No
$(CH_3)_2CO$ – dimethyl ketene*	9.7	1.6	No
CH_2CO – ketene	9.0	0.8	Yes

3.3 Tert-butanol in the dry mixture

In order to examine the effect of the water vapour on the conversion rate of a VOC in the micro-capillary, the tert-butanol was vaporised in dry helium for a concentration of 2650 ppm (± 150 ppm); for this particular experiment, the alcohol concentration (inlet and outlet, regardless the applied voltage) was constant over time.

Figure 5 shows that the conversion rate increases almost linearly when the applied voltage is increased from 3.0 kV up to 8.0 kV. For comparison, the result obtained for the wet mixture at 5.0 kV and C_{in}=2510 ppm (see table 2) is recalled in this figure: the conversion rate is about 10% higher than for the dry mixture. In addition, we have measured the same energy deposited in the plasma for the two mixtures, with or without H_2O, so that the 10% higher rate for the wet mixture cannot be attributed to a difference on the energy input with respect to the dry mixture. On the other hand, the plasma length is sharply reduced when the water vapour is added (see section 2.1), and thus the energy density (Joule/litre) is higher than without H_2O in the gas flow. As a result, production of species acting for the conversion of the tert-butanol should be the highest for the wet mixture.

Same by-products as for the wet mixture were identified, except formaldehyde, methanol, dimethyl ketene, 2-butanone, and [hydroperoxide, 1-methylethyl]. As typical example, time evolution of concentration values for acetone, ketene, acetaldehyde, propyne, and propene, are plotted in figure 6 during the discharge running time (10 min) for 6.0 kV; the concentration for the molecule corresponding to the raw formula C7H14O remains lower (estimated at 7.5 ppm maximum). From the discharge triggering at t=0 min up to t=1.5 min, concentrations increase following the decrease of the concentration of tert-butanol from C_{in}=2580 ppm down to 1830 ppm (not displayed on the figure 6), which value remains constant afterwards until the discharge is stopped. As a results concentrations of by-products remain also rather constant during 8.5 min. Acetone largely dominates all products, as it was also established for the wet mixture, see table 3. For the dry mixture, the percentage of carbon atoms contained in acetone and coming from the converted tert-butanol molecules is 23.5%, which is roughly equal to that obtained for the wet mixture.

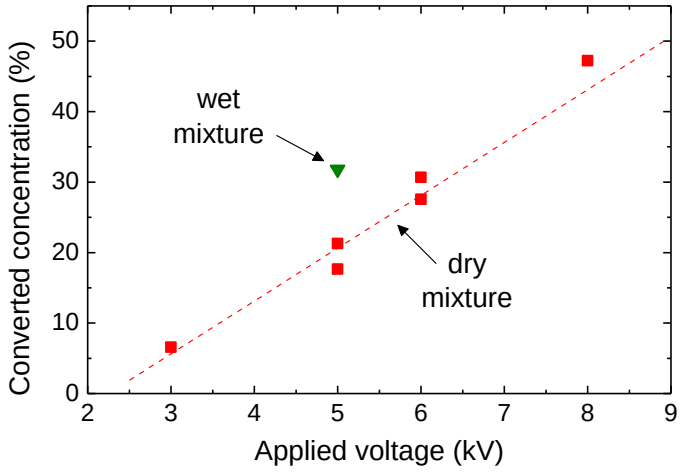

Figure 5 – Conversion rate of tert-butanol for a mean inlet concentration of 2650 ppm (± 150 ppm over 6 experiments) in the dry helium flow, together with the rate for 2510 ppm and 5.0 kV measured for the wet mixture (2.5% H_2O).

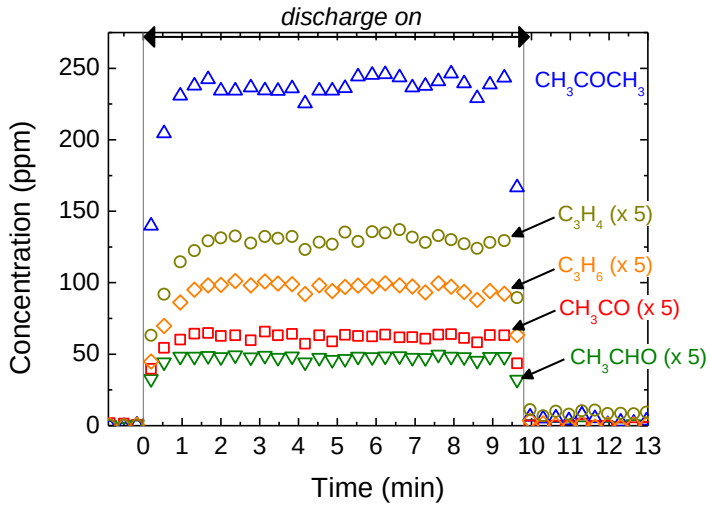

Figure 6 – Time evolution of concentration values for CH_3COCH_3 (up triangles) with those for CH_2CO (squares), CH_3CHO (down triangles), C_3H_4 (circles) and C_3H_6 (diamonds), multiplied by a factor of five. Inlet concentration of tert-butanol: 2580 ppm (±50 ppm), dry mixture, applied voltage: 6.0 kV.

Evolutions of by-products concentrations with respect to the applied voltage are displayed in figure 7. Those of hydrocarbons, propyne and propene, increase when the voltage increases, whereas the concentrations of acetone, ketene, and acetaldehyde tend to reach their maximum value for a voltage higher than 5.0 kV. Moreover, the concentration measured at 8.0 kV for the molecule C7H14O is a factor of 2 lower than that measured for 6.0 kV, although the conversion rate of the tert-butanol grows continuously when the voltage is increased, see figure 5. This emphasises that not only is the injected molecule decomposed by the plasma, but also are some of the by-products coming from this decomposition. In fact, for these products, concentrations measured at the outlet of the micro-capillary necessarily results from a balance between production and loss kinetic processes.

To appear in Journal of Physics D: Applied Physics (2024)

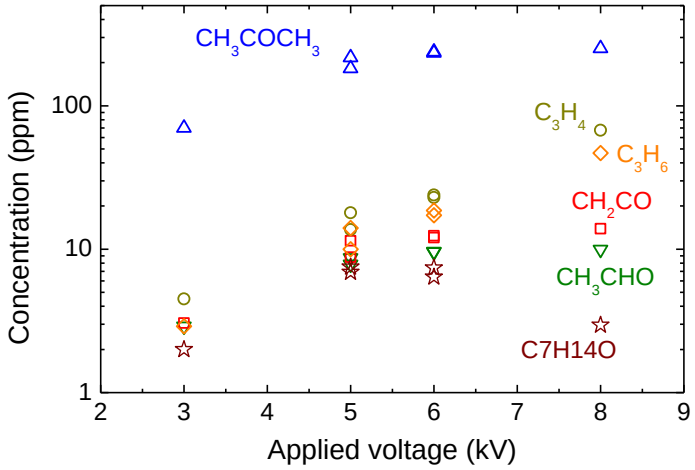

Figure 7 – Concentration of acetone (up-triangles), ketene (squares), acetaldehyde (down triangles), propyne (circles), propene (diamonds), and the molecule corresponding to the raw formula C7H14O (MH^+=115.09 u, stars), measured for 2650 ppm (± 150 ppm) of tert-butanol diluted in helium.

3.4 Methanol and acetone in the wet mixture

CH_3OH and CH_3COCH_3 are compounds detected following decomposition of acetonitrile (methanol) and several alcohols (both). In order to get more information about the effect of the plasma on these molecules, their conversion rates were compared at a fixed applied voltage of 6.0 kV, for inlet concentration values in the range 80 ppm up to 350 ppm diluted in the wet mixture.

Table 4. Conversion rate measured for methanol (CH_3OH) or acetone (CH_3COCH_3) diluted in the mixture He/H_2O(2.5%), for an applied voltage of 6.0 kV.

Molecule	Inlet concentration (ppm)	Outlet concentration (ppm)	Conversion rate (%)
CH_3OH	149.2	41.6	72.1
	225.4	78.2	65.3
	248.1	70.7	71.5
	343.0	98.2	71.4
CH_3COCH_3	81.0	2.5	96.9
	182.0	15.7	91.4

Table 4 emphasises that both CH_3OH and CH_3COCH_3 were removed efficiently from the gas flow, the effect of the plasma being the most important for acetone. As discussed in section 4.2.4, the dissociation of acetone could explain the formation of some of the products identified from the decomposition of tert-butanol.

3.5 Toluene in the wet mixture

The conversion of the aromatic hydrocarbon was studied for an inlet concentration in the range 0.5 ppm up to 5.0 ppm. For that particular experiment, 100 ppmV of toluene (maximum value achievable) was dissolved in the water container. For an applied voltage of 5.0 kV, a conversion rate of 92% (± 4%) was obtained across the entire range of C_{in} values. On top of that, a rate of 46.5% (± 0.5%) was measured at the very low voltage of 1.0 kV and C_{in}=0.8 ppm (± 0.1 ppm). These results emphasize the effectiveness of the plasma to convert aromatic compounds at a very low inlet concentration.

To appear in Journal of Physics D: Applied Physics (2024)

3.6 Global overview for the wet mixture

On figure 8 are plotted the conversion rates of six VOCs belonging to the different chemical families studied in the present work, plotted against the inlet concentration in the micro-capillary tube and diluted in the He/H_2O(2.5%) mixture, and for applied voltage values of 2.0 kV (except for tert-butanol) and 5.0 kV. It highlights that the plasma is able to convert effectively a variety of organic molecules for a wide range of concentration values. For 5.0 kV, the conversion rate can be at least 85% for C_{in} lower than 1000 ppm (all compounds). Logically, it is reduced when the voltage is decreased down to 2.0 kV, but 50% is achieved for a concentration lower than 100 ppm (acetone and isopropanol). Increasing C_{in} above 1000 ppm can induce a drastic reduction of the conversion rate, but this effect strongly depends upon the molecule as it can be seen by comparing results for tert-butanol and acetonitrile at 5.0 kV. On top of that, a very high rate of 95% (±5%) can be reached even at low voltage value, 2.0 kV, for an aromatic compound (toluene) and an inlet concentration lower than 5 ppm.

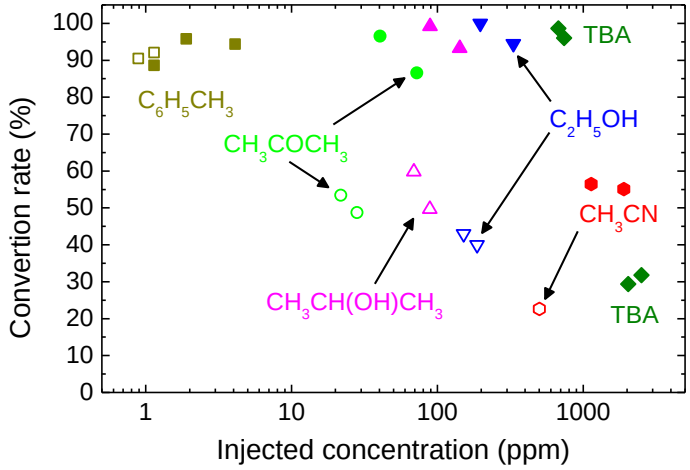

Figure 8 – Conversion rates of ethanol (down triangles), isopropanol (up triangles), tert-butanol (TBA, diamonds), acetone (circles), acetonitrile (hexagons), and toluene (squares), for an applied voltage of 2.0 kV (open symbols) and 5.0 kV (solid symbols). Wet mixtures (2.5% H_2O).

4. Kinetic analysis and discussion

Kinetic processes which are most probably involved in the conversion of the injected VOCs in the micro-capillary plasma are of different types. It is not yet possible to precisely determine the relative importance of each of these processes for the molecules studied in the present work, but a qualitative analysis is at least accessible. In addition, we consider only reactions in the gas phase, without considering processes which could occur on the surface of the tube. As a first step of a more detailed study to be performed in the future, the goal of the following simplified kinetic analysis is to determine whether the presence of the compounds identified at the exit of the capillary tube can be explained by gas phase reactions. In Appendix are listed reactions cited in the text for heavy species, together with their coefficient in the event that this data is known in the literature. Some of them are only suggested in order to get a reasonable explanation of experimental results for tert-butanol; they are not referenced and must be understood as probable processes.

4.1 Removal of the VOCs in dry or wet mixtures

In the first place should be invoked the electron collisions during the propagation of the ionisation wave. Dissociation of the molecules owing to collisions with electrons can occur through excitation of electronic excited states and direct ionisation; dissociative electron attachment can also contribute. Importance of each type of collisions strongly depends upon the corresponding cross sections and the

electron energy distribution function. Ionisation should probably dominates in the streamer head owing to the high value of the corresponding electric field [15]. As a typical example, for iso-propanol it has been shown that the dissociation of the molecule largely dominates over a broad energy range from 10 eV up to 90 eV [37]. Even if the parent ion can be produced, the recombination of this ion with an electron is often a dissociative process [38], thus participating to the removal of the molecule in the discharge afterglow.

On the other hand, important processes concern excited and ionised helium species. Charge transfer reactions can involve He^+ but also the excimer He_2^+ owing to the high pressure of our experiment; this latter ion probably dominates owing to the third body reaction [39],

$$He^+ + 2\,He \rightarrow He_2^+ + He \qquad (R1)$$

Owing to their importance in astrochemistry or in material science, data for acetonitrile, methanol, ethanol, and acetone can be found in the literature. For acetonitrile [40],

$$He^+ + CH_3CN \rightarrow CH_3CN^+ + He \qquad (R2)$$

may be followed by dissociative recombination,

$$e^- + CH_3CN^+ \rightarrow CH_3 + CN(B^2\Sigma^+) \qquad (R3)$$

Also, the dissociative charge transfer from He^+ and producing four types of carbonated ions may be energetically possible [40]; the UMIST database for astrochemistry mentions in particular [41],

$$He^+ + CH_3CN \rightarrow CN^+ + CH_3 + He \qquad (R4a)$$

$$He^+ + CH_3CN \rightarrow CN + CH_3^+ + He \qquad (R4b)$$

For methanol [41],

$$He^+ + CH_3OH \rightarrow OH^+ + CH_3 + He \qquad (R5a)$$

$$He^+ + CH_3OH \rightarrow OH + CH_3^+ + He \qquad (R5b)$$

For ethanol [41],

$$He^+ + C_2H_5OH \rightarrow OH + C_2H_5^+ + He \qquad (R6)$$

And for acetone [41],

$$He^+ + CH_3COCH_3 \rightarrow CH_3CO^+ + CH_3 + He \qquad (R7)$$

Data for the excimer ion are rather scarce, but the following reactions must be mentioned for acetonitrile [42],

$$He_2^+ + CH_3CN \rightarrow CN(B^2\Sigma^+) + CH_3^+ + 2\,He \qquad (R8)$$

Collisions involving the metastable excited state $He(2^3S)$, which is an important energy reservoir (19.8 eV) in helium plasmas, can play also an important role. Following reactions should be considered, firstly Penning ionization (PI),

$$He(2^3S) + M \rightarrow \text{ion products} + He + e^- \qquad (R9a)$$

where, according to the literature, M can stand for acetonitrile [43], methanol [44], or toluene [45], and, secondly, dissociative excitation (DE),

$$He(2^3S) + M \rightarrow \text{neutral products} + He \qquad (R9b)$$

where M can stand for methanol [46]. Obviously, such PI and DE reactions should also take place for acetone, ethanol, iso-propanol, and tert-butanol.

In wet mixtures, the water molecule undergoes dissociative collisions, which are source of hydroxyl radicals or oxygen atoms. Electrons participate to the production of OH and O through several processes [47],

$$e^- + H_2O \rightarrow OH + H + e^- \qquad (R10a)$$

$$e^- + H_2O \rightarrow O(^1D) + H_2 + e^- \qquad (R10b)$$

$$e^- + H_2O \rightarrow OH + H^+ + 2e^- \qquad (R10c)$$

$$e^- + H_2O \rightarrow O(^3P) + H_2^+ + 2e^- \quad \text{(R10d)}$$

$$e^- + H_2O \rightarrow OH + H^- \quad \text{(R10e)}$$

Concerning helium ions, the following reactions should be considered [41, 42],

$$He^+ + H_2O \rightarrow H^+ + OH + He \quad \text{(R11)}$$

$$He_2^+ + H_2O \rightarrow H^+ + OH + 2\,He \quad \text{(R12a)}$$

$$He_2^+ + H_2O \rightarrow HeH^+ + OH + He \quad \text{(R12b)}$$

$$He_2^+ + H_2O \rightarrow H_2^+ + O(^3P) + 2\,He \quad \text{(R12c)}$$

And concerning helium metastable [48],

$$He(2^3S) + H_2O \rightarrow He + OH + H^+ + e^- \quad \text{(R13a)}$$

$$He(2^3S) + H_2O \rightarrow OH + HeH^+ + e^- \quad \text{(R13b)}$$

The metastable state, $O(^1D)$, produced by (R10b), is rapidly quenched down to the ground state, but it reacts also much more efficiently with organic molecules than $O(^3P)$ [49]; in all the followings, 'O' stands for '$O(^3P)$'. On the other hand, the hydroxyl radical is more reactive than the oxygen atom in its ground state at low temperature [50].

Because of all reactions cited above, the efficiency of the micro-capillary helium plasma to remove the studied organic molecules in the wet mixture should be driven by:

- Dissociation of the molecule by electron collisions and production of O and OH by such processes on H_2O in the area where the electric field is the highest, i.e. in the streamer head; production of helium ions and helium metastable states.
- Reactions with He ions and metastables in the plasma column formed by the ionisation wave, which compete with reactions with O and OH coming from the collisions of the water molecule with helium species.

Of course, in the dry mixture, reactions with OH and O cannot be invoked.

4.2 Formation kinetics of by-products

As presented in part 3, the PTR mass spectrometry using H_3O^+ for precursor ion has allowed identification of some by-products following the decomposition of the studied organic molecules, essentially for acetonitrile, ethanol, isopropanol, and tert-butanol. In the followings are detailed the reactions which could explain the formation of these compounds; unless otherwise stated and except for processes involving helium species, all reactions are referenced in the NIST database [50].

4.2.1 Acetonitrile in the wet mixture

The formation of the most populated product, hydrogen cyanide, can be explained considering that dissociation of CH_3CN produces the cyano radical, followed by recombination of CN with the hydrogen atom or reaction with H_2 coming from the dissociation of H_2O,

$$H + CN + He \rightarrow HCN + He \quad \text{(R14)}$$

$$H_2 + CN \rightarrow HCN + H \quad \text{(R15)}$$

Also, presence of propyl cyanide, C_2H_5CN, could be explained by [44]:

$$CN + CH_3CN \rightarrow HCN + CH_2CN \quad \text{(R16)}$$

followed by:

$$CH_3 + CH_2CN \rightarrow C_2H_5CN \quad \text{(R17)}$$

In (R17), the methyl radical can come from various reactions, (R3), (R4a), (R5a), (R9a-b). The production of this radical is also supported by the detection of methanol, which follows the recombination of OH with CH_3,

$$OH + CH_3 + He \rightarrow CH_3OH + He \quad \text{(R18)}$$

4.2.2 Ethanol in the wet mixture

The most populated product is acetaldehyde. This molecule can be produced owing to oxidation reactions of the alcohol, by OH or by O,

$$OH\ (O) + C_2H_5OH \rightarrow CH_3CHOH + H_2O\ (OH) \quad \text{(R19a-b)}$$

$$OH\ (O) + C_2H_5OH \rightarrow CH_2CH_2OH + H_2O\ (OH) \quad \text{(R19c-d)}$$

$$OH\ (O) + C_2H_5OH \rightarrow CH_3CH_2O + H_2O\ (OH) \quad \text{(R19e-f)}$$

followed by radical reactions [50, 52],

$$H + CH_3CHOH \rightarrow H_2 + CH_3CHO \quad \text{(R20)}$$

$$OH\ (O) + CH_3CHOH \rightarrow CH_3CHO + H_2O\ (OH) \quad \text{(R21a-b)}$$

and

$$OH\ (O) + CH_3CH_2O \rightarrow CH_3CHO + H_2O\ (OH) \quad \text{(R22a-b)}$$

In addition, dissociation of C_2H_5OH could produce the ethyl radical, then reacting with the oxygen atom,

$$O + C_2H_5 \rightarrow CH_3CHO + H \quad \text{(R23)}$$

The second important product is acetone, for which the only way to appear should be addition of the methyl to the acetyl radical,

$$CH_3 + CH_3CO \rightarrow CH_3COCH_3 \quad \text{(R24)}$$

These two radicals are coming from the acetaldehyde, which also undergoes the effect of the plasma, i.e.

$$OH\ (O) + CH_3CHO \rightarrow CH_3CO + H_2O\ (OH) \quad \text{(R25a-b)}$$

followed by,

$$H + CH_3CO \rightarrow CH_3 + HCO \quad \text{(R26)}$$

$$O + CH_3CO \rightarrow CH_3 + CO_2 \quad \text{(R27)}$$

On top of that, the methyl radical can also come from the ethyl,

$$H + C_2H_5 \rightarrow CH_3 + CH_3 \quad \text{(R28)}$$

$$O + C_2H_5 \rightarrow CH_2O + CH_3 \quad \text{(R29)}$$

Methanol appears also at a low concentration, following the reaction (R18).

4.2.3 Isopropanol and acetone in the wet mixture

Acetone is the great main by-products for isopropanol. It can result from oxidation reactions producing the 2-hydroxypropyl radical [50, 53], i.e.

$$OH\ (O) + CH_3CH(OH)CH_3 \rightarrow CH_3C(OH)CH_3 + H_2O\ (OH) \quad \text{(R30a-b)}$$

followed by [50, 54],

$$OH\ (O) + CH_3C(OH)CH_3 \rightarrow CH_3COCH_3 + H_2O\ (OH) \quad \text{(R31a-b)}$$

On the other hand, it is known that oxidation processes for acetone are less effective than for alcohols. It was measured that, at the low voltage value of 2.0 kV, the concentration of CH_3COCH_3 at the exit of the micro capillary can be as high as the converted concentration of isopropanol. Thus, loss processes for acetone are quite negligible in such a case. From this, it can be understand that acetone is not so efficiently removed by processes involving helium species, or even by electron collisions, as it can be for other organic molecules. However, it was also found that, when acetone is introduced in the plasma rather than being a decomposition product of another molecule, it is highly removed at high voltage and low concentration values, 6.0 kV and 81 ppm for example, see section 3.4. In such conditions, the influence of helium ions and metastable states could be significant, as well as OH and O coming from dissociation processes of the water molecule. However, more studies are necessary to determine precisely which species are the more important.

4.2.4 Tert-butanol in dry and wet mixtures

At low temperature, the most efficient oxidation reaction of the tert-butanol involves the hydroxyl radical,

$$OH + (CH_3)_3COH \rightarrow (CH_3)_3CO + H_2O \quad \text{(R32a)}$$

$$OH + (CH_3)_3COH \rightarrow (CH_3)_2(CH_2)COH + H_2O \quad \text{(R32b)}$$

Moreover it is known that the tert-butoxy radical rapidly decomposes [55],

$$(CH_3)_3CO \rightarrow CH_3COCH_3 + CH_3 \quad \text{(R33)}$$

so that this latter process is an important source of acetone molecules in the wet mixture. However most of the carbon atoms following the decomposition of $(CH_3)_3COH$ by the plasma are found in acetone either in the dry or in the wet mixture. Thus, the formation of this molecule cannot be explained looking only at the oxidation reactions of the tert-butanol, (R32a-b). It is probable that $(CH_3)_3COH$ is dissociated efficiently by collisions with electrons and helium species, for example to produce the tert-butoxy radical and an hydrogen atom in the case of quenching of the metastable state,

$$He(2^3S) + (CH_3)_3COH \rightarrow (CH_3)_3CO + H + He \quad \text{(R34)}$$

On top of that, as discussed in the previous section, loss processes of acetone are not very efficient so that it is not surprising that this by-product is the most populated at the exit of the micro capillary.

Two hydrocarbons, propene C_3H_6 and propyne C_3H_4, were detected both in dry and wet mixtures. The presence of these molecules in the effluents of the capillary plasma suggests that another possible exit route than (R34) exists for the dissociation of the tert-butanol, i.e. the break of the C-O bound by the helium metastable that produces the tert-butyl radical,

$$He(2^3S) + (CH_3)_3COH \rightarrow (CH_3)_3C + OH + He \quad \text{(R35)}$$

Then, C_3H_6 and C_3H_4 could come from a complicated chain of reactions involving various hydrocarbon radicals, taking into account that $(CH_3)_3C$ and CH_3 (from (R33)) can also undergo dissociative collisions in the plasma. Further studies are necessary to get more insight in such kinetics.

Also detected both in dry and wet mixtures, other compounds containing the oxygen atom are ketene, acetaldehyde, and the molecule with raw formula C7H14O. For this latter, two isomers can tentatively be proposed following the decomposition of either the propene molecule or the acetone one. Indeed, firstly, C_3H_6 can loss the hydrogen atom on the CH group,

$$He(2^3S) + C_3H_6 \rightarrow CH_2CCH_3 + H + He \quad \text{(R36)}$$

while the tert-butanol loss H on a methyl group,

$$He(2^3S) + (CH_3)_3COH \rightarrow (CH_3)_2(CH_2)COH + H + He \quad \text{(R37)}$$

then followed by recombination of produced radicals, giving the [2,4-dimethyl-4-penten-2-ol] molecule,

$$CH_2CCH_3 + (CH_3)_2(CH_2)COH \rightarrow CH_2C(CH_3)CH_2C(CH_3)_2OH \quad \text{(R38)}$$

In the wet mixture, $(CH_3)_2(CH_2)COH$ can also follows from the oxidation reaction (R32b). Secondly, the tert-butanol can loss the hydroxyl radical, see (R35), and acetone can loss the hydrogen atom from one of the methyl group,

$$He(2^3S) + CH_3COCH_3 \rightarrow CH_3COCH_2 + H + He \quad \text{(R39)}$$

followed by radical recombination to form the [2-pentanone, 4,4-dimethyl] molecule,

$$CH_3COCH_2 + (CH_3)_3C \rightarrow (CH_3)_3CCH_2COCH_3 \quad \text{(R40)}$$

Note that (R38) and (R40) must be understood as hypothesis, i.e. there are not referenced in the literature. Taking into account that acetone largely dominates all products in the dry mixture, the formation of ketene and acetaldehyde should follow from the production of the radical CH_3CO, coming from the dissociation process,

$$He(2^3S) + CH_3COCH_3 \rightarrow CH_3CO + CH_3 + He \quad \text{(R41)}$$

which is followed by radical reactions,

$$H + CH_3CO \rightarrow CH_2CO + H_2 \quad (R42)$$

$$CH_3 + CH_3CO \rightarrow CH_2CO + CH_4 \quad (R43)$$

the hydrogen atom and the methyl group coming also from the set (R34-36-37-39) and from (R26-R29, R33) respectively. Acetaldehyde appears owing to the two reactions,

$$HCO + CH_3 \rightarrow CH_3CHO \quad (R44)$$

$$HCO + CH_3CO \rightarrow CH_3CHO + CO \quad (R45)$$

where HCO is coming from (R26). In addition, the acetyl radical is a product of the acetaldehyde reactivity [56],

$$H + CH_3CHO \rightarrow CH_3CO + H_2 \quad (R46)$$

Note that the dissociation of acetone, (R41), is counterbalanced by the recombination reaction (R24). In the wet mixture, the production of the ketene is enhanced by oxidation reactions of the acetyl radical,

$$OH\ (O) + CH_3CO \rightarrow CH_2CO + H_2O\ (OH) \quad (R47a\text{-}b)$$

In addition, the radical HCO is the product of oxidation reactions of the ketene and of the formaldehyde and, as a result, the production of acetaldehyde by (R44-45) should be enhanced in presence of H_2O compared to the dry mixture.

Five molecules were identified only in the wet mixture: CH_2O, CH_3OH, $(CH_3)_2CO$, $C_2H_5COCH_3$, and $(CH_3)_2CHOOH$. Presence of the methanol appears logical owing to the recombination of OH and CH_3 radicals, reaction (R18). On top of that, the formaldehyde is produced by oxidation of the ketene,

$$OH\ (O) + CH_2CO \rightarrow CH_2O + HCO\ (CO) \quad (R48a\text{-}b)$$

or by self-reaction of the formyl radical,

$$HCO + HCO \rightarrow CH_2O + CO \quad (R49)$$

and by the efficient oxidation of the methyl group,

$$O + CH_3 \rightarrow CH_2O + H \quad (R50)$$

The 2-butanone is formed by recombination of the ethyl and acetyl radicals,

$$C_2H_5 + CH_3CO \rightarrow C_5H_5COCH_3 \quad (R51)$$

where C_2H_5 can come from oxidation of the propene molecule [57],

$$O + C_3H_6 \rightarrow C_2H_5 + HCO \quad (R52)$$

Other paths for the formation of C_2H_5 can be linked to the kinetic of the other hydrocarbon radicals, coming from the possible dissociation processes of the tert-butanol, the propyne, and the propene molecules, see for example (R35-36). However, the 2-butanone is not detected in the dry mixture, so that the ethyl radical comes rather from (R52).

No straightforward explanation is found for the formation of [hydroperoxide, 1-methylethyl], $(CH_3)_2CHOOH$, and of dimethyl ketene, $(CH_3)_2CO$. Note that the latter is only a tentative interpretation for the detected ion mass MH^+=71.09 u (exact mass: 71.042 u); however the first is more surely identified by the measured mass MH^+=77.06 u (exact mass: 77.052). It can be noticed that these two compounds contain two methyl groups linked to one carbon atom, so that the same primary specie coming from the dissociation of the tert-butanol molecule, losing at least one methyl group, could be involved in the kinetic path leading to their formation. Moreover, considering that radicals could also undergo dissociation collisions, the following process leading to dimethyl ketene can be suggested,

$$He(2^3S) + (CH_3)_3CO \rightarrow (CH_3)_2CO + CH_3 + He \quad (R53)$$

where the tert-butoxy radical comes from the oxidation reaction of $(CH_3)_3COH$, (R32a).

5. Concluding remarks and perspectives for future works

For the first time, the present work has shown that the non-equilibrium plasma created in a micro-capillary quartz tube (800 µm for internal diameter), owing to a DC-pulsed micro-DBD and the

propagation of an ionisation wave, was able to convert efficiently Volatile Organic Compounds in the gas mixture He/H_2O(2.5%)/VOC at atmospheric pressure. The compounds studied were representatives of organic molecules of different chemical nature: alcohols (methanol, ethanol, isopropanol, tert-butanol), ketones (acetone), nitriles (acetonitrile), and aromatic hydrocarbons (toluene). Conversion of these molecules was studied for a wide range of concentration values, from 1 ppm up to 3000 ppm (depending on the molecule), with the help of high-resolution real-time mass spectrometry (chemical ionisation FTICR BTrap apparatus, using H_3O^+ as precursor ion). It should be noted that the conversion rates measured in the present work are comparable to those obtained in the context of studies of VOC degradation in air flows by more conventional DBDs (i.e. depollution process by large volume filamentary plasmas), although characteristics of these plasmas differ greatly.

Keeping in mind that the use of the hydronium ion did not allow to detect all the molecular species at the micro-tube outlet, the present work emphasises however that a variety of by-products were formed in the plasma. Most of them were detected in the case of tert-butanol, $(CH_3)_3COH$, namely unsaturated hydrocarbons (C_3H_4, C_3H_6), aldehydes (CH_2O, CH_3CHO), alcohol (CH_3OH), ketene (CH_2CO), ketone ($C_2H_5COCH_3$), and possibly dimethyl ketene ($(CH_3)_2CO$), [hydroperoxide, 1-methylethyl] ($(CH_3)_2CHOOH$), and a heavier molecule with raw formula C7H14O. Acetaldehyde was the main product for ethanol, while it was acetone for isopropanol and tert-butanol. On the other hand, hydrogen cyanide (HCN) was dominating in the case of acetonitrile.

These experimental results emphasise that the micro-capillary plasma is able to induce a complex chemical reactivity in the mixture He/H_2O/VOC. For the organic molecules studied, a qualitative analysis of the involved kinetics reveals that helium species (ions and metastable states) and radicals coming from the dissociation of the water molecules (O and OH) are the most probable candidates to explain the formation of all compounds detected by the CI-FTICR apparatus using H_3O^+. However more experiments making use of other ion precursors, like for instance O_2^+ for the detection of saturated hydrocarbons [21], are necessary to achieve a complete description of the plasma reactivity. Complementary measurement methods like FTIR or chromatography are also planned to get more information about by-products resulting from the degradation of the chosen molecules.

Data about quenching reactions of the helium metastable state, He(2^3S), by the VOCs and by radicals (rate constant as well as reaction products) are lacking in the literature and deserve to be precisely determined. However, it can be reasonably suggested that, owing to the high energy value of this state (19.8 eV), the quenching collisions induce dissociation of the organic molecules. On top of that, much well-known oxidation processes by O and by OH should play an important role in wet mixtures. Limited to the gas phase, this kinetic reasoning allows to explain the formation of the great majority of detected by-products (using H_3O^+) coming from the removal of the studied molecules. Nevertheless, it is not yet possible to determine the most important process for this removal. A complete understanding of the plasma reactivity could be achieved by quantitative comparison between experimental results and predictions of a kinetic modelling considering all known physical and chemical processes, starting from electronic collisions on atoms and molecules. However, a reliable modelling requires a precise knowledge of the electric field in the transient plasma (in particular in the streamer head), which can be determined for example by a method based on Stark polarization spectroscopy of He 447 nm line [15]. We plan to address this issue in the future. In addition, the effect of the tube surface on the plasma chemistry cannot be ruled out, that is to say catalytic effects could be involved in the formation of some compounds. Further experimental studies will be necessary to answer this other issue.

6. Appendix

Reactions between heavy species cited in the text. If known, rate coefficients are given in cm^3s^{-1} except for reactions (R1), (R14), (R18) in cm^6s^{-1} and reaction (R33) in s^{-1}, and for a gas temperature equal to 300 K. (*): estimated from data about other radicals. 'S': not referenced in the literature to the authors knowledge, but suggested in order to get a reasonable explanation of experimental results for tert-butanol.

Helium ions reactions			
(R1)	$He^+ + 2\,He \rightarrow He_2^+ + He$	1.4 (-31)	[39]
(R11)	$He^+ + H_2O \rightarrow H^+ + OH + He$	2.0 (-10)	[41]
(R12a)	$He_2^+ + H_2O \rightarrow H^+ + OH + 2\,He$	2.1 (-10)	[42]
(R12b)	$He_2^+ + H_2O \rightarrow HeH^+ + OH + He$	2.1 (-10)	[42]
(R12c)	$He_2^+ + H_2O \rightarrow H_2^+ + O(^3P) + 2\,He$	2.1 (-10)	[42]
(R2)	$He^+ + CH_3CN \rightarrow CH_3CN^+ + He$	unknown	-
(R4a)	$He^+ + CH_3CN \rightarrow CN^+ + CH_3 + He$	1.2 (-9)	[41]
(R4b)	$He^+ + CH_3CN \rightarrow CN + CH_3^+ + He$	1.20 (-9)	[41]
(R8)	$He_2^+ + CH_3CN \rightarrow CN(B^2\Sigma^+) + CH_3^+ + 2\,He$	1.1 (-10)	[42]
(R5a)	$He^+ + CH_3OH \rightarrow OH^+ + CH_3 + He$	1.1 (-9)	[41]
(R5b)	$He^+ + CH_3OH \rightarrow OH + CH_3^+ + He$	1.1 (-9)	[41]
(R6)	$He^+ + C_2H_5OH \rightarrow OH + C_2H_5^+ + He$	3.0 (-9)	[41]
(R7)	$He^+ + CH_3COCH_3 \rightarrow CH_3CO^+ + CH_3 + He$	3.0 (-9)	[41]
Quenching of helium metastable state			
(R13a)	$He(2^3S) + H_2O \rightarrow He + OH + H^+ + e^-$	2.6 (-11)	[48]
(R13b)	$He(2^3S) + H_2O \rightarrow OH + HeH^+ + e^-$	8.5 (-12)	[48]
(R36)	$He(2^3S) + C_3H_6 \rightarrow CH_2CCH_3 + H + He$	S	
(R39)	$He(2^3S) + CH_3COCH_3 \rightarrow CH_3COCH_2 + H + He$	S	
(R41)	$He(2^3S) + CH_3COCH_3 \rightarrow CH_3CO + CH_3 + He$	S	
(R53)	$He(2^3S) + (CH_3)_3CO \rightarrow (CH_3)_2CO + CH_3 + He$	S	
(R34)	$He(2^3S) + (CH_3)_3COH \rightarrow (CH_3)_3CO + H + He$	S	
(R35)	$He(2^3S) + (CH_3)_3COH \rightarrow (CH_3)_3C + OH + He$	S	
(R37)	$He(2^3S) + (CH_3)_3COH \rightarrow (CH_3)_2(CH_2)COH + H + He$	S	
Oxygen atom			
(R50)	$O + CH_3 \rightarrow CH_2O + H$	1.4 (-10)	[50]
(R23)	$O + C_2H_5 \rightarrow CH_3CHO + H$	1.3 (-10)	[50]
(R29)	$O + C_2H_5 \rightarrow CH_2O + CH_3$	2.7 (-11)	[50]
(R52)	$O + C_3H_6 \rightarrow C_2H_5 + HCO$	8.0 (-13)	[57]
(R48b)	$O + CH_2CO \rightarrow CH_2O + CO$	1.3 (-12)	[50]
(R27)	$O + CH_3CO \rightarrow CH_3 + CO_2$	2.6 (-10)	[50]
(R47b)	$O + CH_3CO \rightarrow CH_2CO + OH$	6.4 (-12)	[50]
(R25b)	$O + CH_3CHO \rightarrow CH_3CO + OH$	4.7 (-13)	[50]
(R21b)	$O + CH_3CHOH \rightarrow CH_3CHO + OH$	1.5 (-10)	[50]
(R22b)	$O + CH_3CH_2O \rightarrow CH_3CHO + OH$	3.0 (-12)*	[52]
(R19b)	$O + C_2H_5OH \rightarrow CH_3CHOH + OH$	7.3 (-14)	[50]
(R19d)	$O + C_2H_5OH \rightarrow CH_2CH_2OH + OH$	6.5 (-17)	[50]
(R19f)	$O + C_2H_5OH \rightarrow CH_3CH_2O + OH$	7.0 (-17)	[50]
(R30b)	$O + CH_3CH(OH)CH_3 \rightarrow CH_3C(OH)CH_3 + OH$	6.6 (-14)	[50]
(R31b)	$O + CH_3C(OH)CH_3 \rightarrow CH_3COCH_3 + OH$	8.3 (-11)	[50]

Hydroxyl radical			
(R18)	$OH + CH_3 + He \rightarrow CH_3OH + He$	2.3 (-27)	[50]
(R48a)	$OH + CH_2CO \rightarrow CH_2O + HCO$	8.5 (-12)	[50]
(R47a)	$OH + CH_3CO \rightarrow CH_2CO + H_2O$	7.0 (-11)	[50]
(R25a)	$OH + CH_3CHO \rightarrow CH_3CO + H_2O$	1.6 (-11)	[50]
(R21a)	$OH + CH_3CHOH \rightarrow CH_3CHO + H_2O$	4.0 (-11)*	[52]
(R22a)	$OH + CH_3CH_2O \rightarrow CH_3CHO + H_2O$	3.0 (-11)*	[52]
(R19a)	$OH + C_2H_5OH \rightarrow CH_3CHOH + H_2O$	3.2 (-12)	[50]
(R19c)	$OH + C_2H_5OH \rightarrow CH_2CH_2OH + H_2O$	1.6 (-13)	[50]
(R19e)	$OH + C_2H_5OH \rightarrow CH_3CH_2O + H_2O$	1.6 (-13)	[50]
(R30a)	$OH + CH_3CH(OH)CH_3 \rightarrow CH_3C(OH)CH_3 + H_2O$	5.1 (-12)	[53]
(R31a)	$OH + CH_3C(OH)CH_3 \rightarrow CH_3COCH_3 + H_2O$	5.0 (-11)*	[54]
(R32a)	$OH + (CH_3)_3COH \rightarrow (CH_3)_3CO + H_2O$	1.7 (-13)	[50]
(R32b)	$OH + (CH_3)_3COH \rightarrow (CH_3)_2(CH_2)COH + H_2O$	5.7 (-13)	[50]
Other processes			
(R15)	$H_2 + CN \rightarrow HCN + H$	2.7 (-14)	[50]
(R16)	$CN + CH_3CN \rightarrow HCN + CH_2CN$	unknown	[51]
(R14)	$H + CN + He \rightarrow HCN + He$	1.3 (-30)	[50]
(R28)	$H + C_2H_5 \rightarrow CH_3 + CH_3$	6.0 (-11)	[50]
(R42)	$H + CH_3CO \rightarrow CH_2CO + H_2$	1.9 (-11)	[50]
(R26)	$H + CH_3CO \rightarrow CH_3 + HCO$	3.6 (-11)	[50]
(R46)	$H + CH_3CHO \rightarrow CH_3CO + H_2$	9.0 (-14)	[56]
(R20)	$H + CH_3CHOH \rightarrow H_2 + CH_3CHO$	3.3 (-11)	[50]
(R17)	$CH_3 + CH_2CN \rightarrow C_2H_5CN$	unknown	[51]
(R24)	$CH_3 + CH_3CO \rightarrow CH_3COCH_3$	7.0 (-11)	[50]
(R43)	$CH_3 + CH_3CO \rightarrow CH_2CO + CH_4$	1.0 (-11)	[50]
(R51)	$C_2H_5 + CH_3CO \rightarrow C_5H_5CH_2CO$	3.0 (-11)	[50]
(R38)	$CH_2CCH_3 + (CH_3)_2(CH_2)COH \rightarrow CH_2C(CH_3)CH_2C(CH_3)_2OH$	S	
(R44)	$HCO + CH_3 \rightarrow CH_3CHO$	3.0 (-11)	[50]
(R45)	$HCO + CH_3CO \rightarrow CH_3CHO + CO$	1.5 (-11)	[50]
(R49)	$HCO + HCO \rightarrow CH_2O + CO$	5.0 (-11)	[50]
(R40)	$CH_3COCH_2 + (CH_3)_3C \rightarrow (CH_3)_3CCH_2COCH_3$	S	
(R33)	$(CH_3)_3CO \rightarrow CH_3COCH_3 + CH_3$	4140	[55]

7. Acknowledgments

This work benefited from French 'Future Investments' support from LabEx PALM (ANR-10-LABX-0039-PALM), and from 'Région Ile-de-France' (research project n°16016327 Diagplas – Sésame2016).

8. References

[1] Wengler J, Ognier S, Zhang M, Levernier E, Guyon C, Ollivier C, Fensterbank L and Tatoulian M 2018 Microfluidic chips for plasma flow chemistry: application to controlled oxidative processes *React. Chem. Eng.* **3** 930-941

[2] Lepoetre A, Ognier S, Zhang M, Wengler J, Al Ayoubi S, Ollivier C, Fensterbank L, Duten X and Tatoulian M 2021 Amination of cyclohexane by dielectric barrier discharge processing in a continuous flow microreactor: experimental and simulation studies *Plasma Chem. Plasma Proc.* **41** 351-368

[3] Patinglag L, Sawtell D, Iles A, Melling L and Shaw K 2019 A microfluidic atmospheric-pressure plasma reactor for water treatment *Plasma Chem. Plasma Proc.* 39 561-575

[4] Mizuno A 2013 Generation of non-thermal plasma combined with catalysts and their application in environmental technology *Catal. Today* **211** 2-8

[5] Hossain M, Mok Y S, Wu S, Nguyen V T and Denra A 2022 Effect of metal on corona discharge plasma in a honeycomb catalyst and optimization of the critical parameters for ethylene removal *Appl. Catal. A* **647** 118911

[6] Brandt S, Klute F D, Schütz A, Marggraf U, Drees C, Vogel P, Vautz W and Franzke J 2018 Flexible microtube plasma (FμTP) as an embedded ionization source for a microchip mass spectrometer interface *Anal. Chem.* **90** 10111-10116

[7] Bastin O, Thulliez M, Delchambre A, Devière J, Reniers F and Nonclercq A 2022 Analysis of a nano-pulsed DBD plasma jet for endoscopy and impact of excitation parameters *J. Phys. D : Appl. Phys.* **55** 415204

[8] Zhang H, Zhang J, Xu S, Liu D, Guo L and Li H 2021 Study on the anticancer effects of a 7 μm sized helium plasma jet on micro-tumors *J. Phys. D : Appl. Phys.* **54** 385203

[9] Bashir M, Bashir S, Rees J and Zimmerman W 2014 Surface coating of bonded PDMS microchannels by atmospheric pressure microplasma *Plasma Process. Polym.* **11** 279-288

[10] Robert E, Barbosa E, Dozias S, Vandamme M, Cachoncinlle C, Viladrosa R and Pouvesle J-M 2009 Experimental study of a compact nanosecond plasma gun *Plasma Process. Polym.* **6** 795-802

[11] Xiong Z and Kushner M 2012 Atmospheric pressure ionization waves propagating through a flexible high aspect ratio capillary channel and impinging upon a target *Plasma Sources Sci. Technol.* **21** 034001

[12] Brahme A, Chang Z, Zhao N, Kondeti V and Bruggeman P 2014 Penetration of Ar and He RF-driven plasma jets into micrometer-sized capillary tubes *J. Phys. D : Appl. Phys.* **51** 414002

[13] Gazeli O, Lazarou C, Niu G, Anastassiou C, Georghiou G and Franzke J 2021 Propagation dynamics of a helium micro-tube plasma: Experiments and numerical modeling *Spectr. Acta B* **182** 106248

[14] Ayan H, Yildirim E, Pappas D and Sun W 2011 Development of a cold atmospheric pressure microplasma jet for freeform cell printing *Appl. Phys. Lett.* **99** 111502

[15] Wu S, Lu X, Yue Y, Dong X and Pei X 2016 Effects of the tube diameter on the propagation of helium plasma plume via electric field measurement *Phys. Plasmas* **23** 103506

[16] Gou J, Xian Y and Lu X 2016 Low-temperature, high-density plasmas in long micro-tubes *Phys. Plasmas* **23** 053508

[17] Wu S, Wu F, Liu C, Liu X, Chen Y, Shao T and Zhang C 2019 The effects of the tube diameter on the discharge ignition and the plasma properties of atmospheric-pressure microplasma confined inside capillary *Plasma Process. Polym.* **16** 1800176

[18] Wu S, Guo Y, Ouyang F, Zhou B, Hu B and Cheng H 2023 Characteristics of the plasma sheath in helium discharge within dielectric tubes *Plasma Sci. Technol. 25* 045402

[19] Chiper A, Blin-Simiand N, Heninger M, Mestdagh H, Boissel P, Jorand F, Lemaire J, Leprovost J, Pasquiers S, Popa G and Postel C 2010 Detailed characterization of 2-Heptanone conversion by dielectric barrier discharge in N_2 and N_2/O_2 mixtures *J. Phys. Chem. A* **114** 397-407

[20] Pasquiers S, Heninger M, Blin-Simiand N, Lemaire J, Bauville G, Bournonville B, Louarn E, Jorand F and Mestdagh H 2018 Real-time analysis of toluene removal in dry air by a dielectric barrier discharge using proton transfer reaction mass spectrometry *J. Phys. D : Appl. Phys.* **51** 425201

[21] Thomas S, Blin-Simiand N, Heninger M, Jeanney P, Lemaire J, Magne L, Mestdagh H, Pasquiers S and Louarn E 2020 Direct and real-time analysis in a plasma reactor using a compact FT-ICR MS: degradation of acetone in nitrogen and byproduct formation *J. Am. Soc. Mass Spectrom.* **31** 1579-1586

[22] Trad P, Blin-Simiand N, Jeanney P, Pasquiers S, Lemaire J, Louarn E, Mestdagh H and Heninger M 2023 Monitoring of n-hexane degradation in a plasma reactor by Chemical Ionization

Mass Spectrometry *Analyst* **148** 6050
[23] Ellis A and Mayhew C 2014 *Proton Transfer Reaction Mass Spectrometry: Principles and Applications*. John Wiley & Sons: Chichester, UK.
[24] Smith D and Spanel P 2015 The SIFT and FALP techniques; applications to ionic and electronic reactions studies and their evolution to the SIFT-MS and FA-MS analytical methods *Int. J. Mass Spectrom.* **377** 467-478
[25] Biasioli F, Yeretzian C, Märk T, Dewulf J and Van Langenhove H 2011 Direct-injection mass spectrometry adds the time dimension to (B)VOC analysis *Trends Anal. Chem.* **30** 1003-1017
[26] Guo T, Peng Z, Li X, Zhu H, Xu L, Dong J, Feng J, Cheng P and Zhou Z 2018 Application of proton transfer reaction mass spectrometry for the assessment of toluene removal in a non-thermal plasma reactor *J. Mass Spectrom.* **53** 1126-1134
[27] Li X, Guo T, Peng Z, Xu L, Dong J, Cheng P and Zhou Z 2019 Real-time monitoring and quantification of organic by-products and mechanism study of acetone decomposition in a dielectric barrier discharge reactor *Environ. Sci. Pollut. Res.* **26** 6773–6781
[28] Li X, Li M, Peng Z, Zheng K, Xu L, Dong J, Ren G and Cheng P 2020 Reaction kinetic study of nonthermal plasma continuous degradation of acetone in a closed-loop reactor *Chemosphere* **249** 126215
[29] Guo T, Cheng G, Tan G, Xu L, Huang Z, Cheng P and Zhou Z 2021 Real-time analysis of intermediate products from non-thermal plasma degradation of ethyl acetate in air using PTR-MS: Performance evaluation and mechanism study *Chemosphere* **264** 128430
[30] Sekimoto K, Li S-M, Yuan B, Koss A, Coggon M, Warneke C and de Gouw J 2017 Calculation of the sensitivity of proton-transfer-reaction mass spectrometry (PTR-MS) for organic trace gases using molecular properties *Int. J. Mass Spectrom.* **421** 71–94
[31] Douat C, Kacem I, Sadeghi N, Bauville G, Fleury M and Puech V 2016 Space-time resolved density of helium metastable atoms in a nanosecond pulsed plasma jet: influence of high voltage and pulse frequency *J. Phys. D : Appl. Phys.* **49** 285204
[32] Gazeli K, Bauville G, Fleury M, Jeanney P, Neveu O, Pasquiers S and Santos Sousa J 2018 Effect of the gas flow rate on the spatiotemporal distribution of Ar($1s_5$) absolute densities in a ns pulsed plasma jet impinging on a glass surface *Plasma Sources Sci. Technol.* **27** 065003
[33] Heninger M, Mestdagh H, Louarn E, Mauclaire G, Boissel P, Leprovost J, Bauchard E, Thomas S and Lemaire J 2018 Gas analysis by electron ionization combined with chemical ionization in a compact FTICR mass spectrometer *Anal. Chem.* **90** 7517-7525
[34] Lemaire J, Thomas S, Lopes A, Louarn E, Mestdagh H, Latappy H, Leprovost J and Heninger M 2018 Compact FTICR mass spectrometry for real time monitoring of volatile organic compounds *Sensors* **18** 1415
[35] Buhr K, van Ruth S and Delahunty C 2002 Analysis of volatile flavour compounds by Proton Transfer Reaction-Mass Spectrometry: fragmentation patterns and discrimination between isobaric and isomeric compounds *Int. J. Mass Spectrom.* **221** 1-7
[36] Vanderbrouke A, Morent R, De Geyter N and Leys C 2011 Non-thermal plasmas for non-catalytic and catalytic VOC abatement *J. Hazard. Mat.* **195** 30-54
[37] Vacher J-R, Jorand F, Blin-Simiand N and Pasquiers S 2006 Partial ionisation cross-sections of 2-propanol and ethanol *Chem. Phys.* **323** 587-594
[38] Florescu-Mitchell A and Mitchell J 2006 Dissociative recombination *Phys. Rep.* **430** 277-374
[39] Alves L, Gousset G and Ferreira C 1992 A collisional-radiative model for microwave discharges in helium at low and intermediate pressures *J. Phys. D: Appl. Phys.* **25** 1713-1732
[40] Ito H, Onitsuka S and Koshimura K 2012 Analysis of dissociative excitation reactions of CH_3CN with the ECR plasmas of Ar and He *Diam. Relat. Mat.* **24** 111-115
[41] McElroy D, Walsh C, Markwick A, Cordiner M, Smith K and Millar T 2013 The UMIST database for astrochemistry 2012 *Astron. Astrop.* **550** A36 - http://www.udfa.net
[42] Binns W and Ahl J 1978 Excitation and quenching reactions in E-beam excited He/H_2O and

He/CH_3CN systems *J. Chem. Phys.* **68** 538-546

[43] Pasinszki T, Yamakado H and Ohno K 1995 Penning ionization of CH_3CN and CH_3NC by collision with He*(2^3S) metastable atoms *J. Phys. Chem.* **99** 14678-14685

[44] Yamakado H, Yamauchi M, Hoshino S and Ohno K Penning ionization of CH_3OH, $(CH_3)_2O$, and $(CH_3CH_2)_2O$ by collision with He*(2^3S) metastable atoms *J. Phys. Chem.* **99** 17093-17099

[45] Kishimoto N, Matsumoto M, Matsumura E Ohno K 2006 Collision-energy-resolved Penning ionization electron spectroscopy of toluene and chlorotoluenes *Eur. Phys. J. D* **38** 75-84

[46] Yu H, Gu Y, Sun G, Yin Y, Li X, Shen G and Wang L 1994 Dissociative excitation of CH_3N0_2 and CH_30H by collisions with metastable helium in the beam experiment *Chem. Phys. Lett.* **230** 243-248

[47] Budde M, Cunha Dias T, Vialetto L, Pinhao N, Guerra V and Silva T 2022 Electron-neutral collision cross sections for H_2O: I. Complete and consistent set *J. Phys. D: Appl. Phys.* **55** 445205

[48] Sanders R and Muschlitz 1977 Chemiionization and secondary ion reactions in H_2O and D_2O *Int. J. Mass Spectrom.* **23** 99-108

[49] Schofield K 1978 Rate constants-108 for the gaseous interactions of $O(2^1D_2)$ and $O(2^1S_0)$ – A critical evaluation *J. Photochem.* **9** 55-68

[50] Manion J, Huie R, Levin R, Burgess Jr. D, Orkin V, Tsang W, McGivern W, Hudgens J, Knyazev V, Atkinson D, Chai E, Tereza A, Lin C-Y, Allison T, Mallard W, Westley F, Herron J, Hampson R and Frizzell D NIST Chemical Kinetics Database, NIST Standard Reference Database 17, Version 7.0 (Web Version), Release 1.6.8, Data version 2015.09, National Institute of Standards and Technology, Gaithersburg, Maryland, 20899-8320. Web address: https://kinetics.nist.gov/

[51] Koeta O, Blin-Simiand N, Faider W, Pasquiers S, Bary A and Jorand F 2012 Decomposition of acetaldehyde in atmospheric pressure filamentary nitrogen plasma *Plasma Chem. Plasma Proc.* **32** 991-1023

[52] Magne L, Pasquiers S, Gadonna K, Jeanney P, Blin-Simiand N, Jorand J and Postel C 2009 OH kinetic in high-pressure plasmas of atmospheric gases containing C_2H_6 studied by absolute measurement of the radical density in a pulsed homogeneous discharge *J. Phys. D : Appl. Phys.* **42** 165203

[53] Atkinson R, Baulch D, Cox R, Hampson R, Kerr J, Rossi M and Troe J 1999 Evaluated Kinetic and Photochemical Data for Atmospheric Chemistry, Organic Species: Supplement VII *J. Phys. Chem. Ref. Data* **28** 191-393

[54] Magne L, Blin-Simiand N, Gadonna K, Jeanney P, Jorand J, Pasquiers S and Postel C 2009 OH kinetics in photo-triggered discharges used for VOCs conversion *Eur. Phys. J.: Appl. Phys.* **47** 22816

[55] Curran H 2006 Rate constant estimation for C1 to C4 alkyl and alkoxyl radical decomposition *Int. J. Chem. Kinet.* **38** 250-275

[56] Baulch D, Cobos C, Cox R, Frank P, Hayman G, Just Th, Kerr J, Murrells T, Pilling M, Troe J, Walker R and Warnatz J 1995 *J. Phys. Chem. Ref. Data* **24** 1609-1603
Erratum: same authors (1994) *J. Phys. Chem. Ref. Data* **23** 847-1033

[57] Atkinson R 1997 Gas-phase tropospheric chemistry of volatile organic compounds: 1. alkanes and alkenes *J. Phys. Chem. Ref. Data* **26** 215–290